第33卷 第3期
2012年3月

焊 接 学 报
TRANSACTIONS OF THE CHINA WELDING INSTITUTION

Vol. 33 No. 3
March 2012

超低碳超高强 X120 管线钢焊接热影响区粗晶区的组织转变

雷玄威[1]， 王红鸿[1]， 尹雨群[2]， 赵晋斌[2]， 钱 勇[1,3]， 吴开明[1]

（1. 武汉科技大学 国际钢铁研究院，武汉 430081；2. 南京钢铁集团有限公司，南京 210035；
3. 巨龙钢管有限公司，南京 210035）

摘 要：采用热模拟试验方法分析了超低碳超高强 X120 管线钢焊接热影响区粗晶区的组织转变. 粗晶区连续转变曲线（SH-CCT）表明，在较宽的冷却速度范围内（0.8 ~ 25 ℃/s），X120 管线钢粗晶区组织为贝氏体；当冷却速度小于 0.8 ℃/s 和大于 25 ℃/s 时，分别有少量准多边形铁素体和少量马氏体形成. 热模拟焊接热输入在 12 ~ 25 kJ/cm 的范围时，粗晶区组织为贝氏体；硬度（276 ~ 297 HV 0.2）与室温冲击吸收功（208 ~ 225 J）稳定. 结果表明，X120 管线钢可适用较大范围热输入的焊接，这主要与超低碳设计有关.

关键词：管线钢；焊接热影响区；组织转变；贝氏体；热模拟
中图分类号：TG113 文献标识码：A 文章编号：0253 - 360X（2012）03 - 0073 - 04

雷玄威

0 序 言

用于运输石油天然气的管线钢，从 20 世纪 70 年代开始投入使用 X65，80 年代 X70 钢被引入工程建设，20 世纪 90 年代末生产出 X80 钢管，一直到目前研制的 X100 和 X120 钢，其强度逐渐发展到1 000 MPa 以上. 使用超高强管线钢可以降低建设高压输气管线的成本，从总体上节省 5% ~15%，还可以提高输送天然气的效率，节省运行费用[1,2]，是当前及未来管线钢发展的要求和趋势.

X120 管线钢的研制由埃克森美孚公司开始于 1993 年，要求高强与高韧性的结合，但同时也要考虑到良好的焊接性能和结构的完整性. 为达到高强高韧性的结合，X120 管线钢的显微组织设计为复相组织或贝氏体组织[3-5]. 为使管线钢具有良好的焊接性能，焊接热影响区具有匹配的强度、良好的抗裂韧性和抗氢致裂纹敏感性[4]，要求 X120 超高强管线钢具有低的碳当量和抗氢裂纹指数[6,7]. 此外，为使其具有结构的完整性，对该钢的焊接工艺也有新的要求. 目前 X120 超高强管线钢处于研制阶段，有必要对该钢在焊接热循环下的焊接热影响区组织转变进行分析，从而对焊接性能做出准确的评价，为 X120 钢成分的优化、合适焊接工艺的选择提供技术数据.

文中采用热模拟对热影响区粗晶区的组织转变进行了分析，得到 X120 焊接热影响区 SH-CCT 曲线，以及 X120 焊接热影响区组织转变的特点. 同时对模拟的不同焊接热输入下的粗晶区的力学性能进行了分析.

1 试验方法

试验材料为南京钢铁公司研制的 X120 超高强管线钢，生产工艺为控制轧制工艺（TMCP 工艺）. X120 超高强管线钢是在超低碳（0.04% ~0.06%）及低硫的基础上，添加 Nb，Ti，Ni，Mo，V，Cr 等合金元素，从而获得的一种细晶粒高强度合金钢.

采用热模拟试验测定 SH-CCT 曲线. 试验设备为 Gleeble 3500. 试样尺寸为 ϕ 6 mm × 85 mm. 热模拟工艺：测定 A_{c_1} 和 A_{c_3} 相变温度点，升温速率为 200 ℃/h，峰值温度为 1 000 ℃，空冷；测定不同冷却速度下的组织转变，升温速率为 280 ℃/s，峰值温度为 1 350 ℃，峰值温度停留时间为 1 s，冷却时从峰值温度先以 40 ℃/s 冷却到 A_{c_3} 温度，再分别以 12 个不同冷却速率冷却到 200 ℃，然后空冷. 得到在不同热模拟工艺下的热膨胀曲线，根据热膨胀曲线测得相变点.

收稿日期：2011 - 03 - 14
基金项目：国家自然科学基金重点资助项目（50734004）

采用热模拟试验模拟焊接热影响区粗晶区组织并测定冲击韧性. 试样尺寸为 75 mm × 10.5 mm × 10.5 mm. 升温速率为 280 ℃/s,峰值温度为 1 350 ℃,峰值温度停留时间为 1 s. 模拟焊接热输入分别为 12,15,18,21,25 kJ/cm(对应模拟的 $t_{8/5}$ 分别为 5.7,8.7,12.9,17.5,24.2 s).

将热模拟试验后的试样磨平、抛光、用 4% 硝酸酒精腐蚀,采用光学显微镜进行观察分析. 采用扫描电镜对冲击断口形貌进行观察分析. 将模拟不同热输入下焊接热影响区粗晶区的组织进行维氏硬度测试,并将试样加工成 55 mm × 10 mm × 10 mm 的尺寸,进行冲击韧性测试.

2　试验结果与分析

2.1　相转变温度

根据各个不同工艺下的热膨胀曲线,测定冷却过程中各相变点. 相变起始温度与结束温度均取曲线拐点值. 测得不同冷却速度下的相变起始与结束温度,见表 1. 测得相变 A_{c_1} 温度为 713 ℃,A_{c_3} 温度为 871 ℃. 钢的 B_S 点经计算约为 570 ℃.

表 1　SH-CCT 的相变起始与结束温度

Table 1　Phase transformation starting and finishing temperature

冷却速度 v/(℃·s^{-1})	相变起始温度 T_s/℃	相变结束温度 T_f/℃
0.1	623	502
0.4	584	514
0.8	571	495
1.6	542	455
3.1	533	434
6.3	507	426
10.0	520	436
12.5	496	437
19.4	490	419
25.0	487	426
40.0	479	390
60.0	483	399

2.2　连续冷却组织观察与分析

X120 超高强管线钢的显微组织以上贝氏体为主[5]. 维氏硬度值约为 310 HV 0.2. 图 1 为不同冷却速度下的显微组织形貌. 当冷却速度为 0.1 ℃/s 时,组织以粒状贝氏体(GB)为主,伴以少量的准多边形铁素体(F). 粒状贝氏体中含有大量的 M-A 组元,呈条状或岛状分布于铁素体基体上. 冷却速度为 0.4 ℃/s 时得到粒状贝氏体和微量准多边形铁素体. 粒状贝氏体中的 M-A 组元尺寸变小,呈细小的岛状. 冷却速度为 0.8 ℃/s 时得到粒状贝氏体和微量准多边形铁素体,并开始有条状的上贝氏体(UB)形成. 粒状贝氏体 M-A 组元减小. 冷却速度为 1.6 ℃/s 时得到粒状贝氏体和板条状上贝氏体. 粒状贝氏体显著减少,大量板条状上贝氏体出现. 随着冷却速度从 3.1 ℃/s 增加到 19.5 ℃/s,组织主要是板条状上贝氏体,粒状贝氏体逐渐减少,直至消失. 冷却速度为 25 ℃/s 时,仍以板条状上贝氏体为主,但开始有马氏体(M)组织形成,数量很少; 随着冷却速度增大到 40 ℃/s 和 60 ℃/s,马氏体组织的数量逐渐增加.

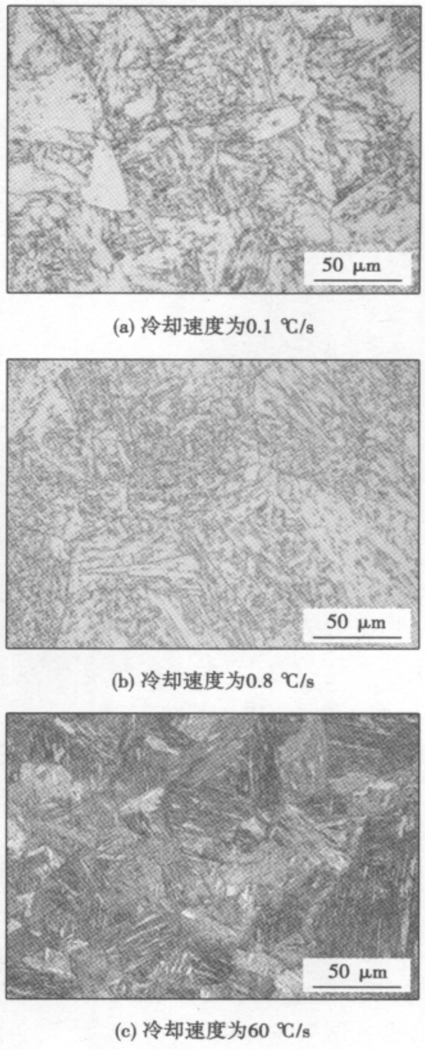

图 1　不同冷却速度下的显微组织形貌

Fig. 1　Microstructures with different cooling rates

2.3　组织连续转变曲线

根据热膨胀曲线、显微组织分析,绘制出 X120 超高强管线钢的 SH-CCT 曲线,见图 2. 从图 2 中可以看出,X120 管线钢热模拟得到的主要是贝氏体组

织. 当冷却速度较小时，主要组织是粒状贝氏体. 当冷却速度较大时，主要组织是板条状上贝氏体. 当 $t_{8/5} \leqslant 12$ s 时得到马氏体组织；当 $t_{8/5} \geqslant 370$ s 时得到先共析铁素体组织. 同时从图 2 可以看到，即使冷却速度很大（达到 60 ℃/s）也只形成了少量的马氏体组织.

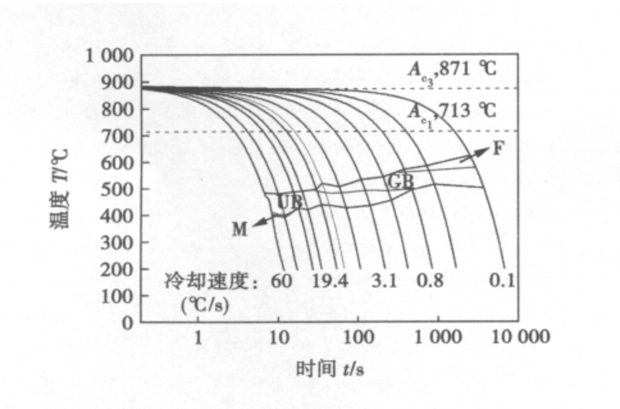

图 2　X120 管线钢的 SH-CCT 曲线

Fig. 2　SH-CCT diagram of pipeline steel X120

板条状上贝氏体中铁素体板条细小、分布均匀，铁素体周围细小的富碳相在一定程度上也可提高韧性，板条状上贝氏体不但强度高，而且韧性也好，即具有良好的综合性能，是一种较理想的组织. 粒状贝氏体组织中，在颗粒状或针状铁素体基体中分布着许多 M-A 小岛，这些小岛可以起到复相强化作用，使粒状贝氏体表现出较好的强韧性，因而 X120 管线钢表现出了优异的焊接性能. 图 3 为 SH-CCT 的显微组织比例关系曲线.

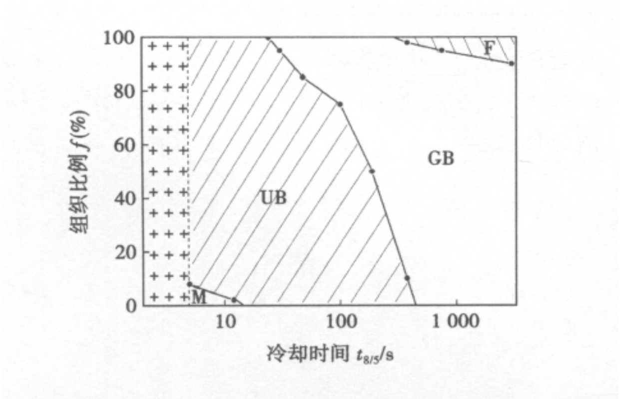

图 3　显微组织连续转变比例关系曲线

Fig. 3　Microstructures fraction of SH-CCT

2.4　焊接热影响区粗晶区显微组织与力学性能

在热模拟焊接热输入为 12 ~ 25 kJ/cm 的范围内，热影响区粗晶区的显微组织主要为上贝氏体，且晶粒尺寸大小变化不大，平均晶粒尺寸约为 40 μm. 表 2 为力学性能测试结果. 硬度测试结果表明，室温组织硬度在 276 ~ 297 HV 0.2 之间，变化不大，与显微组织分析相吻合. 室温冲击试验表明冲击吸收功的平均值在 208 ~ 225 J 之间，且冲击值非常稳定. 冲击断口形貌如图 4 所示，有明显的韧窝存在，且韧窝较深，为韧性断裂.

表 2　力学性能试验结果

Table 2　Mechanical properties tests results

热输入 $E/(\mathrm{kJ \cdot cm^{-1}})$	硬度（HV 0.2）	冲击吸收功 $A_{\mathrm{KV}(20\ ℃)}$ /J
12	$\frac{280, 313, 298}{297}$	$\frac{221, 233, 217}{224}$
15	$\frac{278, 271, 283}{277}$	$\frac{202, 221, 234}{219}$
18	$\frac{306, 288, 278}{291}$	$\frac{228, 221, 204}{218}$
21	$\frac{275, 278, 274}{276}$	$\frac{197, 208, 218}{208}$
25	$\frac{294, 277, 288}{286}$	$\frac{228, 217, 229}{225}$

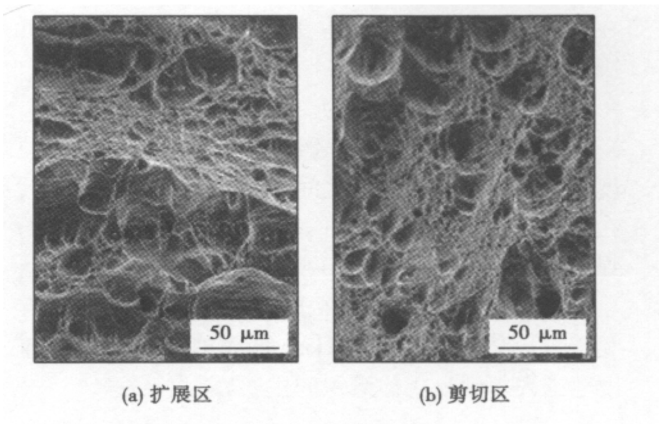

图 4　冲击断口形貌（18 kJ/cm）

Fig. 4　Fracture surfaces of impacted specimen

3　讨　　论

在冷却速度很慢时，碳从奥氏体晶内向晶界处扩散，从而在奥氏体晶界处形成了富碳区，随温度的降低而成为了残留的 M-A 组元. 因为钢中碳的含量非常低，所以形成的 M-A 组元含量也非常少，且因冷却速度造成的碳扩散速度的不同，形成的M-A 组元的含量也不同. 同时冷却速度很慢时，奥氏体内合金元素有充足的时间进行扩散，同时合金元素 Mn，Si，Ni，Cr 的加入在一定程度上起到了稳定奥氏体、推迟先共析铁素体形成的作用，少量的准多边形先共析铁素体在原奥氏体晶界慢慢形成并长大，直

到温度进入到下一个组织转变温度区间.

进入到下一个组织转变温度区间时,碳的扩散决定了其组织的转变. 一方面奥氏体组织转变成铁素体组织发生碳的扩散,另一方面碳的扩散因钢中强碳化物元素 Nb,Ti 等的加入而受到影响变慢,于是发生了不完全的扩散转变. 粒状贝氏体的形成依赖于两个因素,连续冷却和低碳含量[8]. 文中在很宽的冷却速度范围内得到粒状贝氏体组织,超低碳设计是主要原因. 超低碳设计提高了贝氏体的转变温度,有利于贝氏体的形成,从而提高钢的强韧性. 冷却速度渐渐变大时,相变直接进入到贝氏体转变区. 但由于贝氏体转变温度区间停留时间缩短,贝氏体铁素体没有充足时间长大,形成了板条状,即板条状上贝氏体. 当冷却速度较大时(达到25 ℃/s),原奥氏体组织开始进入到马氏体转变温度区间,开始形成马氏体组织.

4 结 论

(1) X120 超高强管线钢的 SH-CCT 曲线表明,在很宽的冷却速度范围内 X120 管线钢能得到以贝氏体为主的组织.

(2) 在焊接热输入为 12~25 kJ/cm 的范围内,X120 焊接热影响区粗晶区组织为上贝氏体组织,硬度在 276~297 HV 0.2 之间,室温冲击吸收功稳定,在 208~225 J 之间,表明 X120 管线钢具有良好的焊接性能.

(3) 超低碳含量提高了贝氏体的转变温度,有利于贝氏体的形成,是 X120 管线钢在很宽冷却速度范围内得到贝氏体组织的主要原因.

参考文献:

[1] Corbett K T, Bowen R R, Petersen C W. High strength steel pipeline economics [C] // The International Society of Offshore and Polar Engineers. Proceeding of the Thirteenth International Offshore and Polar Engineering Conference. USA, Honolulu, Hawaii, 2003: 105-112.

[2] Liu Wenyan, Wang Lai, Liu Jibin, *et al*. Microstructures and properties in simulated heat-affected zones of 685 MPa grade copper-bearing steel [J]. Journal of Iron Steel Research, International, 2007,14(5): 220-226.

[3] Asahi H, Hare T, Sugiyama M, *et al*. Development of plate and seam welding technology for X120 lineipe [C] // The International Society of Offshore and Polar Engineers. Proceeding of the Thirteenth International Offshore and Polar Engineering Conference. USA, Honolulu, Hawaii, 2003: 19-25.

[4] Koo J K, Luton M J, Bangaru N V, *et al*. Metallurgical design of ultra-high strength steels for gas pipelines [C] // The International Society of Offshore and Polar Engineers. Proceeding of the Thirteenth International Offshore and Polar Engineering Conference. USA, Honolulu, Hawaii, 2003: 10-18.

[5] Guo Aimin, Misra R D K, Xu Jinqiao, *et al*. Ultrahigh strength and low yield ratio of niobuium-microalloyed 900 MPa pipeline steel with nano/ultrafine bainitic lath [J]. Materials Science and Engineering A, 2010, 527(16/17): 3886-3892.

[6] Hillenbrand Hans-Georg, Liessem Andreas, Biermann Karin, *et al*. Development of high strength material and pipe production technology for grade X120 line pipe [C] // Proceedings of IPC 2004. International Pipeline Conference. Canada, Calgary, Alberta, 2004: 1-7.

[7] Graf M K, Hillenbrand H G, Heckmann C J, *et al*. High-strength large-diameter pipe for long-distance high pressure gas pipelines [C] // The International Society of Offshore and Polar Engineers. Proceeding of the Thirteenth International Offshore and Polar Engineering Conference. USA, Honolulu, Hawaii, 2003: 97-104.

[8] Bhadeshia H K D H. Bainite in steels [M]. 2nd Edition. London: The Institute of Materials, 2001.

作者简介: 雷玄威,男,1987年出生,硕士研究生. 主要从事金属材料焊接工艺与组织控制的研究. Email: dewonlxw@126.com

通讯作者: 吴开明,男,博士,教授. Email: wukaiming@wust.edu.cn

FEM simulation of mechanical controlling parameters for type IV cracking on P91 steel weld ZHANG Jianqiang[1,2], LUO Changhong[2], ZHANG Yinglin[2] (1. State Key Laboratory of Advanced Welding and Joining, Harbin Institute of Technology, Harbin 150001, China; 2. School of Power and Mechanical Engineering, Wuhan University, Wuhan 430072, China). pp 57 – 60, 64

Abstract: The maximum principal stress, von Mises equivalent stress and equivalent creep strain of the welded joint of martensitic heat-resistant steel (P91) was simulated by FEM under the condition of 600 ℃ and 80 MPa. The results show that the maximum principal stress and von Mises equivalent stress are high on the curved points of two sides of groove faces near the fine grain HAZ. The creep strain mainly concentrates in the fine grain HAZ, the maximum creep strain locates in the bottom of fine grain HAZ of the specimen. The stress triaxiality is maximum in the fine grain HAZ and creep cracking occurs because of the intensive constrain of the base metal and weld. The simulation results are in well agreement with the experimental results of crack initiation site and propagation path by using the stress triaxiality as the mechanically controlling parameter of the martensitic heat-resistant steel weld. Therefore, it is reasonable for the stress triaxiality to be used for analyzing the initiation and propagation of type IV cracking in the fine grain HAZ.

Key words: martensitic heat-resistant steel, type IV cracking; von Mises equivalent stress; equivalent creep strain; numerical simulation

Microstructure and wear resistance of (Ti,Nb)C reinforced composite coating in-situ synthesized by argon arc cladding WANG Yongdong, LI Bairu, WANG Shuhua, LIU Xing (Department of Material Science and Technology, Heilongjiang Institute of Science and Technology, Harbin 150022, China). pp 61 – 64

Abstract: Ni-based reinforced composite coating was prepared on the surface of 16Mn steel by means of argon arc cladding technique with the pre-alloyed powders of Ni60A, Nb, Ti and C. The microstructure of the composite coating was examined with OM, SEM and XRD, and the abrasion property of the coating was measured under different loads. The results showed that metallurgical bonding between the coating and the substrate occurred without defects like pores and cracks. The microstructure of the composite coating consisted of (Ti,Nb)C particles, γ-Ni austenite dendrites and $Cr_{23}C_6$ eutectics. With the increase of load at room temperature, the weight loss during abrasion of the composite coating increased slowly, whereas that of 16Mn steel increased remarkably. The wear resistance of the composite coating was 11 times higher than that of the substrate.

Key words: argon arc cladding; composite coating; in-situ synthesis; wear resistance

Analysis on microstructure of in-situ synthesis TiC-M_7C_3 ceramic hard phase LIU Zhengjun, LI Lecheng, ZONG Lin, SU Yunhai (School of Materials Science and Engineering, Shenyang University of Technology, Shenyang 110870, China). pp 65 – 68

Abstract: TiC-M_7C_3 ceramic hard phases were in situ synthesized using plasma arc surfacing technology. The morphology and distribution of TiC-M_7C_3 hard phases in the surfacing layer was investigated with the X-ray diffraction (XRD), optical microscope (OM), scanning electron microscope (SEM) and spectrum analyzer (EDS). Rockwell hardness tester and wet sand abrasion tester were used to examine the performance of the surfacing layer. The results show that the microstructure of the surfacing layer consists of high-carbon martensite and a large number of ceramic hard phases, for example, TiC and M_7C_3, which disperse in the matrix of surfacing layer. The hardness of the surfacing layer is 66.4 HRC and the weight reduction is 0.086 g. TiC can act as the nuclei of M_7C_3 to improve the nucleation rate of M_7C_3 ceramic hard phases and grain refinement. The Fe-Cr-Ti-C surfacing layer has higher hardness and better wear resistance than Fe-Cr-C alloy due to the combined effect of TiC and M_7C_3 ceramic hard phases.

Key words: ceramic hard phase; surfacing layer; in-situ synthesis; wear resistance

Effects of pulse frequency on TCGMAW droplet transfer modes XIE Shengmian[1,2], WU Kaiyuan[1], WEN Yuanmei[1,3], GE Weiqing[1], HUANG Shisheng[1] (1. School of Mechanical & Automotive Engineering, South China University of Technology, Guangzhou 510641, China; 2. School of Information and Communication Engineering, Guangzhou Maritime College, Guangzhou 510725, China; 3. Information Engineering College, Guangdong University of Technology, Guangzhou 510006, China). pp 69 – 72

Abstract: The effects of pulse frequency on TCGMAW (Twin-wire Co-pool Gas-shielded Metal Arc Welding) droplet transfer modes and weld appearances were investigated with high-speed photography and wavelet analysis. Under the welding parameters in this paper, the droplet transfer mode of the front wire was spray transfer and that of the back wire was projected transfer when the pulse frequency was high (140 Hz); the droplet transfer mode of both the front and back wires was projected transfer when the pulse frequency was low (40 Hz); the droplet transfer mode of both the front and back wires was spray transfer when the pulse frequency was moderate (60 – 100 Hz); the droplet transfer of both the front and back wires was one-droplet-per-pulse when the pulse frequency changed between 40 Hz and 140 Hz; and the weld appearances were preferable when the pulse frequency changed between 60Hz and 100 Hz.

Key words: TCGMAW; droplet transfer; high-speed photography; wavelet analysis; weld appearance

Microstructure transformation of coarse-grained region in heat-affected zone during welding of ultra-low carbon ultra-high strength pipeline steel LEI Xuanwei[1], WANG Honghong[1], YIN Yuqun[2], ZHAO Jinbin[2], QIAN Yong[1,3], WU Kaiming[1] (1. International Research Institute for Steel Technology, Wuhan University of Science and Technology, Wuhan 430081, China; 2. Nanjing Iron & Steel Group Co., Ltd., Nanjing 210035, China; 3. Julong Steel Pipe Co., Ltd., Nanjing 210035, China). pp 73 – 76

Abstract: The microstructure transformation of coarse-grained region in heat-affected zone (CG-HAZ) during welding of an ultra-high strength X120 pipeline steel was investigated with thermal simulation. Simulated HAZ continuous cooling transformation (SH-CCT) curves showed that the bainitic microstructure was obtained in CG-HAZ in a wide cooling rate range (0.8 – 25 ℃/s). Besides bainite, a small proportion of quasi polygongal ferrite formed in CG-HAZ when the cooling rate was lower than 0.8℃/s whereas a small proportion of martensite formed when the cooling rate was higher than 25 ℃/s. Bainite was obtained in the CG-HAZ when the welding heat input was in the range of 12 – 25 kJ/cm. The Vickers hardness of CG-HAZ (276 – 297 HV0.2) and the impact toughness at room temperature (208 – 225 J) was stable. Simulated results indicated that the X120 pipeline steel was suitable for welding with wide heat inputs, which was attributed to the ultra-low carbon design.

Key words: ultra-high strength pipeline steel; heat-affected zone; microstructure transformation; bainite; thermal simulation

Mathematical model and simulation for cutting of pipe tee with root face groove WANG Qihua, YIN Guofu, XU Lei, HE Saisong (School of Manufacturing Science & Engineering, Sichuan University, Chengdu 610065, China). pp 77 – 80

Abstract: Aimed at the groove cutting during the pipe tee manufacturing, this paper compared bevel groove with root face groove, and presented the advantages of root face groove cutting for pipe tee. The principle of root face groove cutting for branch pipe and main pipe was demonstrated, and then the root face groove cutting model was established, based on the bevel groove cutting model. After simulation with AutoCAD VBA programming tools, the models were verified to be reliable and practical. This paper provides a new approach to improve the welding quality and enhance the manufacturing efficiency of pipe tee.

Key words: CNC pipe cutting; pipe tee; bevel groove; root face groove

New half-bridge soft-switching CO_2 inverter welding machine SHE Zhiting[1], CAO Da[1], XIA Fuping[2], LI Ying[1] (1. College of Electrical and Information Engineering, Hunan University, Changsha 410082, China; 2. Central Research Institute, Sany Group Co., Ltd., Changsha 410100, China). pp 81 – 84

Abstract: In order to reduce the switching loss and ripple of output voltage of CO_2 inverter welding machine and realize the digital control, the soft-switching commutation principle of half-bridge DC-DC converter with adding two assistant power switches to DC busline side is analyzed in this paper. Based on ARM-controlled and double closed-loop (current and voltage) control strategy, a full digital CO_2 inverter welding machine is designed. The soft-switching commutation of new half-bridge DC-DC converter is simulated in the Matlab/Simulink environment. The experimental results illustrate that the full digital ARM-controlled new half-bridge soft-switching inverter welding machine has significant advantages over the traditional analog-controlled inverter welding machine, such as low switching loss, low voltage ripple, flexible programming ability and better stability.

Key words: CO_2 inverter welding machine; half-bridge DC-DC converter; soft-switching; digital control

Analysis of brazed joints between carbon fiber reinforced SiC composite and titanium alloy with TiC CUI Bing, HUANG Jihua, XIONG Jinhui, ZHANG Hua (School of Materials Science and Engineering, University of Science and Technology Beijing, Beijing 100083, China). pp 85 – 88

Abstract: Carbon fiber reinforced SiC (C_f/SiC) composite was successfully joined to titanium alloy with Ag-Cu-Ti-(Ti + C) mixed powder under proper parameters. The interfacial microstructure was examined with scanning electron microscope (SEM), energy dispersive spectrometer (EDS) and X-ray diffraction (XRD), and the mechanical properties of the brazed joints were tested. The results showed that Ti in the powder reacted with the composite during brazing, the resultant joints mainly consisted of TiC, Ti_3SiC_2, Ti_5Si_3, Ag, TiCu, Ti_3Cu_4 and Ti_2Cu phases. The dense bonding layers formed and were reinforced by TiC in situ synthesized from the reaction between C and Ti in the filler materials. The TiC particulates obviously relieved the thermal stress in the heterogeneous joint, resulting in an increase in shear strength of the brazed joint. The maximum shear strengths of the brazed joints at room temperature, 500 ℃ and 800 ℃ reached 145 MPa, 70 MPa and 39 MPa, respectively, which were remarkably higher than those brazed with C_f/SiC/Ag-Cu-Ti/TC4.

Key words: C_f/SiC composite; Ti alloy; brazing; TiC

Reactive contact brazing between aluminium alloy and copper by high frequency induction method ZHANG Hongtao, LIU Duo, FENG Jicai, HU Leliang (School of Materials Science and Engineering, Harbin Institute of Technology (Weihai), Weihai 264209, China). pp 89 – 92

Abstract: High-frequency induction contact reactive brazing of 6063 aluminium alloy to pure copper was investigated in this paper. The composition of the brazing flux was optimized according to the brazing process and mechanical properties of the resultant joints. The interfacial microstructure and phase constitution of the joint was analyzed by means of SEM and EDS. The results showed that the joint made with the flux of 65% $ZnCl_2$ + 10% NaCl + 25% NH_4Cl was better than the joints made with the other two fluxes. The thickness of the brazing seam was about 80 μm and the interface mainly consisted of Al solid solution and Al_2Cu phases, and massive Zn and Na elements diffused into the seam. The maximum shearing strength of the joint reached 58 MPa.

Key words: aluminium alloy; pure copper; contact reactive brazing; interfacial structure

Effect of sodium molybdate on corrossion behavior of 2024 and its weld joint by FSW SHEN Changbin[1,2], CHEN Ying[1], GE Jiping[1,2] (1. Liaoning Key Materials Laboratory for Railway, Dalian Jiaotong University, Dalian 116028, China; 2. School of Materials Science and Engineering, Dalian Jiaotong University, Dalian 116028, China). pp 93 – 96

Abstract: In this paper, 2024 aluminum alloy was friction stir welded. In the ambient mixed solution of 0.2 mol/L $NaHSO_3$ and 0.6 mol/L NaCl with the addition of different concentrations of sodium molybdate (Na_2MoO_4), the effect of Na_2MoO_4 on the corrosion behavior of the friction stir weld and